Pharmaceutical Research, Vol. 26, No. 5, May 2009 (© 2009)
DOI: 10.1007/s11095-009-9828-z

Research Paper

An Investigation into the Rheology of Pharmaceutical Inter-granular Material Bridges at High Shear Rates

Barry Crean,[1,2,3] Xinyong Chen,[1] Simon R. Banks,[2] Walter G. Cook,[2] Colin D. Melia,[3] and Clive J. Roberts[1,4]

Received July 4, 2008; accepted January 7, 2009; published online February 3, 2009

Purpose. This study was undertaken to investigate the rheological properties of inter-granular material bridges on the nano-scale when strained at high shear rates.
Materials and Methods. Atomic force microscopy (AFM) was used as a rheometer to measure the viscoelasticity of inter-granular material bridges for lactose:PVP K29/32 and lactose:PVP K90 granules, produced by wet granulation.
Results. The loss tangent (tan δ) and both the storage (G') and loss shear moduli (G'') of inter-granular material bridges were measured as a function of the probe–sample separation distance, oscillation frequency and relative humidity (RH). As the probe was withdrawn from the granule surface tan δ initially increased rapidly from zero to a plateau phase. G'' became increasingly dominant as the bridge was further extended and eventually exceeded G'. At high RH, capillary forces were foremost at bridge rupture, whereas at low RH elastic forces dominated. The effect of increasing frequency was to increase the effective elasticity of the bridge at high RH.
Conclusions. AFM has been employed as a rheometer to investigate the nano-scale rheology of inter-granular material bridges. This novel method may be used to obtain a fundamental understanding how different binders, granulated with different diluent fillers, behave at high shear rates.

KEY WORDS: atomic force microscope; bridges; granulation; nano-scale; rheology.

INTRODUCTION

Granulation is a progressive size enlargement process, in which a binder is used to develop adhesion between individual particles, enabling nucleation and growth of a larger agglomerate, a granule. One of the challenges in the pharmaceutical industry is to generate a precise understanding of granulation processes, so that manufacturing conditions and formulation properties may be predicted and optimised (1). It is perceived that a greater fundamental knowledge of the dynamics of particle-particle and particle-fluid interactions may allow prediction of macroscopic powder/granule properties and thereby enable more rigorous control of the granulation process (1,2). The purpose of our work was to develop a novel method for the investigation of the rheological properties of inter-granular material bridges at high strain rates (e.g., a high frequency of shear) at the nano-scale.

Modelling the viscoelastic properties of materials is a complex exercise arising out of the impact of a number of factors. Hence, the mechanical models of viscoelastic materials have been derived assuming specific constraints (3) for example in ignoring adhesion, in not accounting for contact geometry or quantifying such a geometry as the contact area that monotonically increases during a large amplitude loading cycle (4).

In this work we apply dynamic AFM measurements to measure the rheological properties of inter-granular material bridges on the nano-scale. The Voigt spring and dashpot model is applied to measure the loss tangent (tan δ) of inter-granular material bridges formed at elevated RH, as a spherical probe is withdrawn from the granule surface. This model also provides a qualitative measurement of the loss

[1] Laboratory of Biophysics and Surface Analysis, School of Pharmacy, The University of Nottingham, Nottingham, NG7 2RD, UK.
[2] AstraZeneca Charnwood PAR&D, Bakewell Road, Loughborough, LE11 5RH, UK.
[3] Formulation Insights, School of Pharmacy, The University of Nottingham, Nottingham, NG7 2RD, UK.
[4] To whom correspondence should be addressed. (e-mail: clive.roberts@nottingham.ac.uk)

ABBREVIATIONS: AFM, atomic force microscope; APDD, amplitude-phase-deflection distance curve; *c*, cantilever deflection; cos, cosine; *d*, probe detected spatial position; $\dot{d}$, velocity of probe; $\ddot{d}$, acceleration of probe; d_0, cantilever length when static; d_1, cantilever forced amplitude; *D*, Voigt model dashpot dampening coefficient; E_{adh}, energy of adhesion; G', storage modulus (elastic properties); G'', loss modulus (viscous properties); Hz, Hertz; *K*, Voigt model spring restoring coefficient; *k*, spring constant of an AFM cantilever; MW, molecular weight average; n, number of experiments; nm, nanometre; Pa, Pascal; PVP, polyvinyl pyrrolidone; RH, relative humidity; *s*, probe–granule separation distance; sin, sine; tan δ, loss tangent; *z*, *z* piezo drive detected spatial position; z_0, original position of z-piezo; z_1, *z*-piezo drive amplitude; $\dot{z}$, velocity of *z*-piezo drive; $\ddot{z}$, acceleration of z piezo drive; θ, cantilever oscillation signal phase lag; φ, phase lag of AFM deflection signal; ω, angular velocity.

and storage moduli (G' and G'') as a function of the probe–granule separation distance. Viscoelastic data for two different granule formulations, being lactose:PVP K29/32 and lactose:PVP K90, are compared.

BACKGROUND THEORY

Dynamic viscoelastic measurements were performed by introducing a high frequency (50–1,000 Hz), but low amplitude (~3 nm) oscillation to the system. A piezo-induced oscillation (drive amplitude), at frequencies much lower than the resonant frequency of the cantilever, results in a 'forced' oscillation of the cantilever when in contact with granule surface. The amplitude, phase and deflection signals of the cantilever were simultaneously monitored using a laser beam and a position-sensitive photodiode. Differences between drive and forced amplitude and phase signals depend on the viscoelastic properties of the intervening sample.

A model for a linear viscoelastic material may be derived assuming a sample and instrument to be a 'black box' composed of elastic (storage), viscous (loss) and inertia components (Fig. 1). This model is usually termed a Voigt model (5) and full derivations are detailed in the Appendix. G' and G'' may be derived as:

$$G' = \frac{k}{b}\frac{\gamma\cos\varphi - \gamma^2}{1 - 2\gamma\cos\varphi + \gamma^2} \tag{1}$$

$$G'' = \frac{k}{b}\frac{\gamma\sin\varphi}{1 - 2\gamma\cos\varphi + \gamma^2} \tag{2}$$

where k is the cantilever spring constant (N m^{-1}), b is a geometry correction factor, θ is the mechanical lag between force and displacement, and γ denotes the ratio of drive to cantilever amplitudes. It follows that tan δ may be defined as:

$$\tan\delta = \frac{G''}{G'} = \frac{\sin\varphi}{\cos\varphi - \gamma} \tag{3}$$

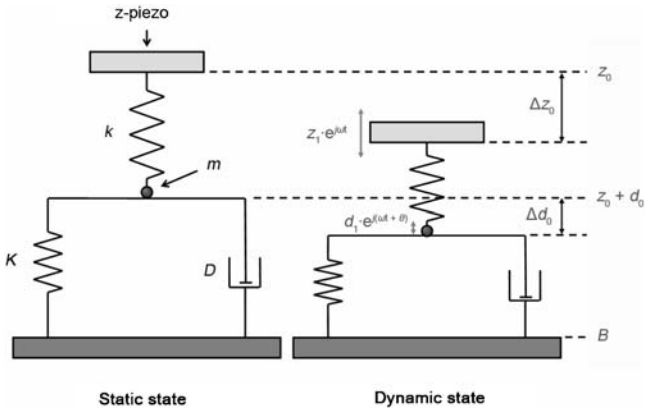

Fig. 1. Schematic of Voigt spring and dashpot model. A cantilever of spring constant (k) driven at amplitude z, oscillates at an amplitude d when brought into contact with a viscoelastic sample. The viscoelastic sample consists of a viscous component (D) and an elastic component (K).

It should be noted from Eq. 3 that tan δ is independent of the cantilever spring constant and probe geometry and so it is on this parameter that quantitative analysis will be based. Work reported here differs from previous work (3,5–7) in that it is the cantilever and not the sample which is subjected to an oscillatory drive. In addition, this model does not account for adhesion forces. Choi and Kato (8) have added an extra spring in parallel with the existing Voigt model in order to incorporate the meniscus force formed when the probe is withdrawn from the sample surface. Consequently, G'' is calculated as before and the storage modulus was derived as:

$$G' = \frac{k}{b}\frac{\psi\cos\varphi - \psi^2}{1 - 2\psi\cos\varphi + \psi^2} + k_m \tag{4}$$

where k_m is the slope of the force distance curves as function of separation distance. The application of this more complex model does not alter the interpretation of the data presented in this work and hence has not been applied here (see example in Appendix comparing data processed by both models).

MATERIALS AND METHODS

α-Lactose monohydrate, (Pharmatose® 450 M) was a gift from DMV International (Holland) and polyvinyl pyrrolidone (PVP), Povidone® grades K29/32 and K90, were donated by ISP (Germany).

Granules were produced using a Kenwood CH180 mixer (Kenwood Ltd, UK). Excipients were first pre-screened through a 500 μm mesh size sieve (Endecotts Ltd., UK). The weighed excipients (Mettler AT200 balance, Mettler Toledo, UK), consisting of 3% *w*/*w* binder, were then placed into a Kenwood CH180 granulator bowl which was used to prepare the granules (50 g). Powders were blended dry for 2 min at speed 1 with a tip speed ≈ 16.4 m s^{-1} ≈ 3,400 rpm as measured by a laser tachometer (RS Components Ltd., UK). Water was then added by hand at 1 ml min^{-1} using a syringe with a needle bore size of 0.8 mm. Identical binder levels (3% *w*/*w*), saturation levels (14% *w*/*w*) and kneading times (6 min) were used for both formulations. Wet granules were screened through a 1.4 mm sieve and left to dry in an oven (Gallenkamp Plus II Oven, Weiss-Gallenkamp, UK) at 50°C overnight. Dried granules were then passed through a 1 mm sieve.

Granule particle size distributions were measured using a Mastersizer 2000 laser diffractometer fitted with a Scirocco dry powder feeder (Malvern Instruments Ltd., UK). Triplicate samples of approximately 1 g were fed into the diffractometer at a vibration feed rate of 70% and a dispersive air pressure of 2 bar. Background readings were recorded (10,000 background snaps over 10 s) prior to measurement readings being taken at 20,000 measurement snaps for 20 s.

The ambient moisture content of the granules was determined in triplicate using a MB45 moisture analyser balance (Ohaus, UK). Samples (~1 g) were heated on disposable aluminium pans from ambient temperature to 105°C over 3 min using a linear temperature ramp. Samples were then held at this temperature until the change in sample

mass was less than a 1 mg over 2 min; this endpoint was automatically detected by the apparatus.

The granule batches were separated into representative samples using a spinning riffler splitter (Microscal Ltd., UK). All subsequent analyses were performed on these split samples. Granules were stored in double-sealed, clean, dry amber glass bottles at room temperature.

Scanning electron microscopy (SEM) of granule morphology was performed using a Jeol JSM 6060LV microscope (JEOL (UK) Ltd, UK). The granules were gold coated at 30 mA for 3 min under vacuum prior to image analysis (SCD 030, Balzers, UK). SEM analysis was carried out under high vacuum at an accelerating voltage of 12 kV with a spot size of 55 nm.

Atomic Force Microscopy (AFM) measurements were undertaken using an EnviroScope® AFM (Veeco Metrology Inc., CA, USA) equipped with a Nanoscope IIIa® controller and an environment chamber. The measurements were performed at ambient temperature (25°C) and RH was controlled between 20% and 80% RH, with an accuracy of 0.1%. The humidity was controlled and maintained as a constant air supply to the sample chamber, facilitated by a Triton Laboratory Instrument Control Application, version 1.0.32 (Triton Technology Ltd., UK). Granules were carefully mounted onto a steel stub using Araldite resin (Bostik Fendling Ltd., UK) before insertion into the sample chamber.

AFM Cantilever Calibration and Modification

Silicon tapping mode cantilevers (OTESPA®, Veeco), with resonant frequencies of 300–400 kHz, were used to obtain frequency-dependent viscoelastic measurements. The spring constant (k) of each OTESPA cantilever was established by the Sader method (9), applying a correction factor of 0.7 (10). The spring constants of the OTESPA cantilevers were measured to be 0.25–0.35 N m^{-1} and 40–60 N m^{-1} respectively. In order to avoid sample damage, and to ensure constant contact geometry, the OTESPA cantilever probe geometry was altered to a well-defined spheroid form. The spherical probes were constructed by attaching borosilicate microspheres (Duke Scientific Corporation, Fremont, CA, USA), 20±2 μm in diameter, to the apex of the cantilever with Loctite 350 UV curing adhesive glass bond (Henkel Loctite Adhesives Ltd., UK). This was achieved by means of a previously reported procedure (11) using a Nanoscope IIIa® MultiMode® AFM (Veeco). Prior to data collection, probes were cleaned using a UV tip cleaner (BioForce Nanosciences Inc., IA, USA) for 20 min to remove organic contaminants from the glass probe surface.

Cantilevers were imaged by SEM in order to ensure that the borosilicate microspheres had been successfully attached to the cantilever apex and to accurately measure the diameter of the spherical probe. SEM analysis was undertaken at low vacuum using an accelerating voltage of 14 kV and a spot size of 51 nm.

Following completion of each experimental run the cantilevers again underwent SEM analysis to ensure that the experiment had neither unduly affected the microsphere shape nor removed the microsphere completely from the AFM cantilever.

Pseudo-Static Adhesion Force Measurements

Pseudo-static normal force-distance (n=75) curves were measured between the colloid probe (i.e., OTESPA cantilever with sphere attached at apex) and the surface of a lactose: PVP granule, over a sampling area of 1 μm^2 (with a distance of 500 nm between sampling points) as a function of RH. Measurements were taken at 20%, 40%, 60% and 80% RH after samples were equilibrated at the required RH for 40 min. Equilibrium granule moisture content was achieved after a conditioning time of 30 min at each target RH. This was established by Dynamic Vapour Sorption (Surface Measurement Systems Ltd., UK) analysis. Prior to data collection, force–distance curves were also measured against a freshly cleaned borosilicate glass cover-slip, which was used as a non-indenting reference to determine the sample deformation. The borosilicate cover slip was cleaned using a Piranha solution [a mixture of 30% H_2O_2 and 70% concentrated H_2SO_4 (1:4)] at ambient temperature. The treated cover slip was then rinsed with HPLC grade water (Millipore®), isopropranol, and finally dried in a stream of nitrogen gas.

Dynamic Force Measurements

In the dynamic force measurement, the 'amplitude' data are obtained from the root of mean square (RMS) value of the deflection signal while the 'deflection' (or 'TM deflection') data are deduced from the mean value of the deflection signal. The experimental geometry used to perform the viscoelastic measurements is illustrated in Fig. 2. Amplitude–phase–deflection–distance (APDD) curves were measured at a constant oscillation amplitude (~0.2 V) and at fixed frequencies (50, 100, 500 and 1,000 Hz) as a function of RH and the probe–granule separation distance. Measurements were not performed outside this range of frequencies as amplitude signals could not be measured at lower frequencies, due to exceeding the band width limits of the instrument, whilst undesired cantilever resonant effects appeared at higher frequencies. The extension includes a Quadrex Extender allowing accurate phase measurement. The Nanoscope was upgraded with additional Analogue Digital Converter channels by Veeco, which permitted the amplitude, deflection and phase signals to be simultaneously measured when used in tapping mode. An in-built lock-in amplifier, incorporated within the Quadrex extender unit, was used to collect APDD curves, which were measured at a constant ramp velocity of 20 nm s^{-1}. The z-scanner piezo was used to oscillate the cantilever, as insufficient piezo–cantilever coupling was achieved when the piezo of the tip holder designed for use in liquids alone was used to oscillate the cantilever.

The APDD signals were calibrated by measuring APDD curves against a 'stiff' borosilicate glass cover-slip which was cleaned using the aforementioned procedure. This freshly cleaned surface was used as a non-indenting reference to determine linear relationship between the cantilever deflection and the detector's electronic export. At each oscillation frequency, after the probe was in contact with the substrate surface, the drive amplitude value which yielded a constant amplitude signal of ~0.2 V in the compliance region of the APDD curve was noted. Similarly, the drive phase parameter which resulted in a constant 'baseline' phase shift signal of 0° at

each frequency of oscillation was recorded. Using these parameters the APDD curves were then measured between the probe and the surface of a granule. As the stiff borosilicate surface was considered to be non-compressible in comparison with the weak atomic force microscope cantilever, the phase shift measured on the borosilicate was solely due to the piezo transducer and atomic force microscope electronics, and the amplitude of the cantilever was equal to the piezo amplitude. These assumptions ignored errors that may have occurred due to slip of the probe on the surface.

APDD curves were first obtained at 80% RH and then at 20% RH in order to investigate the effect of hydration on inter-granular material bridges. Data were collected using the same positions on the surface of the granule for each value of oscillation frequency and RH.

The Voigt model was applied to data in order to investigate inter-granular material bridge properties as a function of oscillation frequency and RH. The unloading APDD profile, where the inter-granular material bridge was formed, was employed for analysis.

RESULTS

The water content of the lactose:PVP K29/32 and lactose:PVP K90 granules were similar (3.92±0.18% and 3.85±0.01% *w*/*w* respectively) and the size distributions for both formulations are illustrated in Fig. 3. Both distributions were bimodal, although PVP K29/32 yielded a lower proportion of fines (granules less than 100 μm in diameter) than PVP K90; this was most likely due to more efficient spreading of the less viscous polymer grade. The mean granule size was approximately 250 μm, which is generally regarded as an optimal granule product attribute. The granules formed were approximately spherical in shape and the original lactose particles could be identified from the agglomerates (Fig. 4). Fig. 5 shows an example of a borosilicate microsphere successfully attached to the apex of a cantilever.

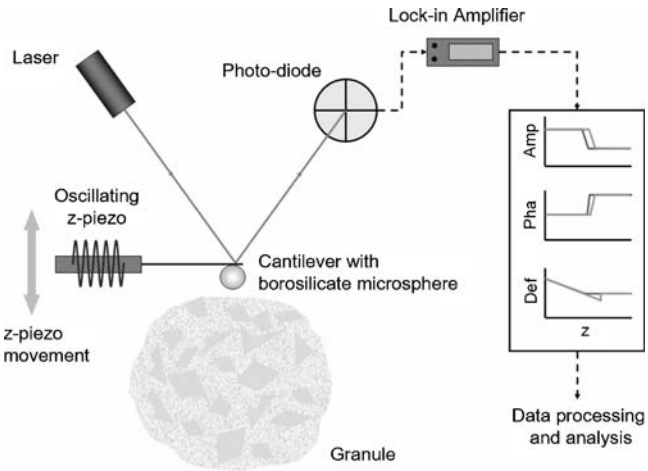

Fig. 2. Experimental geometry used to investigate the nano-rheology of inter-granular material bridges relating to pharmaceutical granules. Modifications were made to a commercial AFM system to obtain the frequency-dependent viscoelastic data. The *z*-scanner was used to impose a sinusoidal drive of small amplitude (~3 nm) onto the cantilever. A lock-in amplifier was used to detect the amplitude and the phase of the cantilever response.

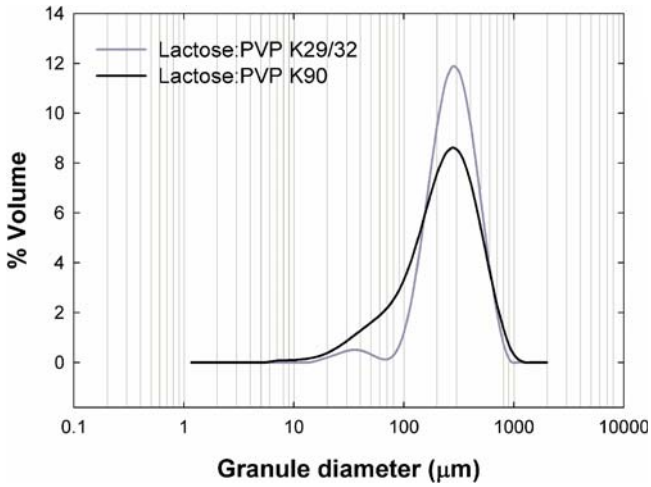

Fig. 3. Size distributions of lactose:PVP granules made by high shear wet granulation (n=3).

Pseudo-Static Adhesion

The effect of relative humidity on the energy of adhesion (E_{adh}) between a borosilicate microsphere colloid probe and

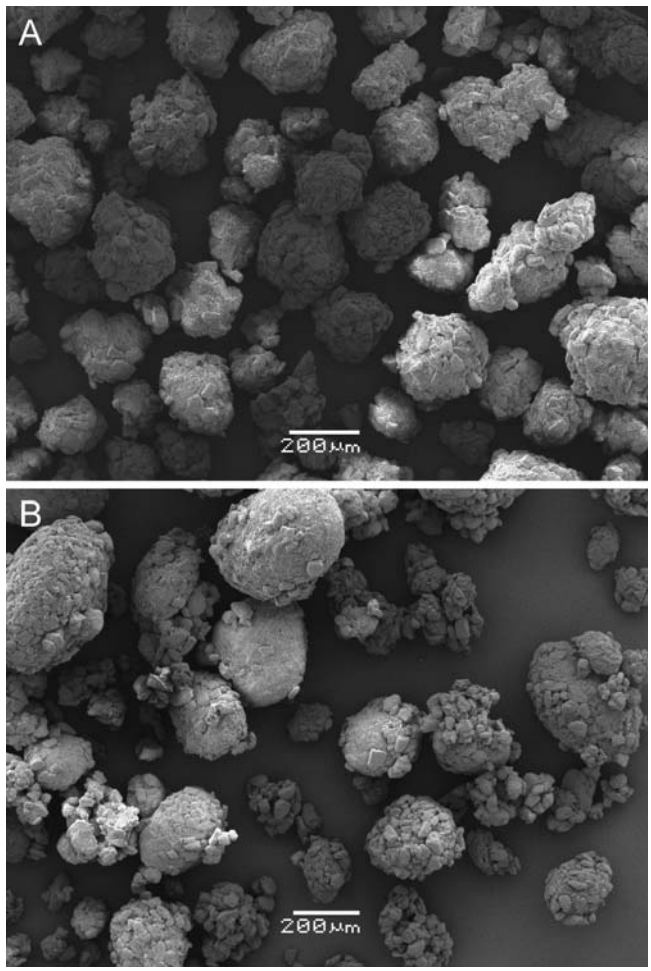

Fig. 4. SEM images of both granule formulations, being lactose:PVP K29/32 (**A**) and lactose:PVP K90 (**B**).

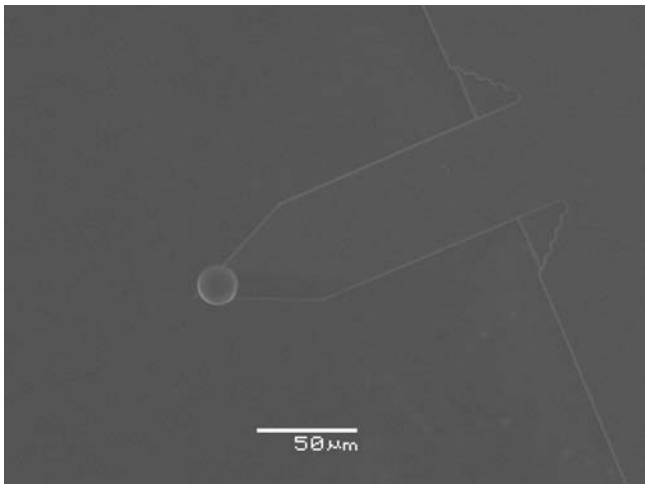

Fig. 5. SEM image of borosilicate microsphere attached to the end of a tapping mode cantilever.

the surface of a granule is shown in Fig. 6. Granule surfaces were elastic at 20–60% RH and the colloid probe abruptly left the granule surface upon withdrawal, indicating a low E_{adh} (assessed via the area enclosed within the hysteresis observed in the force data (12)) (Fig. 6). At a critical RH of 80% a viscous bridge was formed between the colloid probe and the granule surface as the water plasticised the polymeric binder (Fig. 6). At vapour pressures of 20–40% the adhesion event ceased abruptly at a distance of ~20 nm from the granule surface; this indicated that the granule surface was elastic. However, at 60% RH the E_{adh} began to increase even though the force–distance profiles resembled those measured at lower RH. The length of adhesion was much greater at 80% RH (~200 nm) due to the capillary forces. This observation, in addition to the shape of the force–distance curves, suggests that at 80% RH pliable bridges were formed as it took longer for the bridge to break, as predicted by conventional viscoelastic behaviour.

Dynamic Viscoelastic Measurement Data Analysis

The relationship between the simultaneously measured amplitude, phase and deflection signals and the probe–sample separation distance is illustrated in Fig. 7. When the probe was not in direct contact with the surface, there was no change in cantilever deflection (as it was being driven at a frequency well below its resonant frequency). Therefore, before contact with the sample, the amplitude signal was zero, the phase signal was meaningless and the deflection signal was constantly at the free level (Fig. 7 A). As the probe was driven towards the granule surface it first made intermittent contact with the surface as the probe continues to move away from the surface for part of its oscillation cycle (B), and then completely contacted the surface (C) before indenting the surface of the granule (D). Upon contact the piezo–cantilever coupling increased which facilitated cantilever oscillation. As the probe was withdrawn from the surface a material bridge, subjected to oscillatory shear, was formed between the probe and the granule surface (C–E). The formation of this viscous bridge resulted in an increase in adhesion (as shown by the deflection signal) and mechanical cantilever phase lag. The bridge ruptured upon further withdrawal of the probe (E) and the probe finally returned to its original position away from the surface of the granule (A). A reference point set as 0 nm on the separation axis was taken as the point at which the probe fully contacted the surface (C); values of separation less than zero represent the compliance region of the curves where the probe indented the granule surface and values greater than zero represent the probe position as it is withdrew away from the surface (unload). The Voigt model was only applied to the unloading curves at positive distances of separation where material bridges were formed. The hysteresis observed in all signals (Fig. 7) showed that an adhesion event had occurred.

Voigt Model

The Voigt model is valid when γ, the ratio of drive to cantilever amplitudes, is less than 1. This is based on the premise that piezo–cantilever coupling is at a maximum when the probe is in contact with a purely elastic surface and that the oscillation frequency is well below the cantilever's resonant frequency. However, an increased amplitude signal, which exceeded that measured on the glass surface, was consistently observed in APDD curves measured on granule surfaces, and therefore the Voigt model could not be applied to the whole profile of the unloading APDD curves. Such an elevated amplitude signal may have resulted from lateral sliding of the large spherical probe on the granule surface, or enhanced coupling between the probe and surface, or both. Consequently, the G' and G'' profiles were meaningless between maximum sample indentation and where $\gamma>1$: this point was generally ~20–30 nm away from the granule surface. In order to redress this, the maximum amplitude value and the corresponding phase value, taken from APDD curves measured on the granules, were used as the reference values from which γ (which as a result was always less than 1) and φ were calculated.

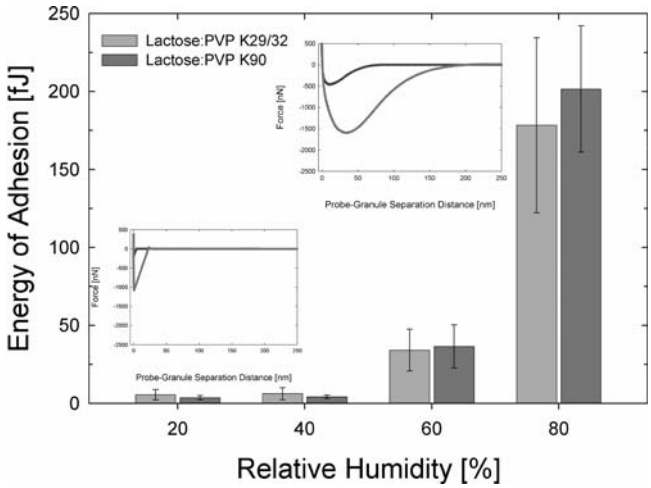

Fig. 6. Effect of RH on energy of adhesion between a colloidal glass probe and lactose:PVP granules. At a critical RH of 80% a viscous bridge is formed in contrast to elastic adhesions at lower RH values (n=75; mean±SD).

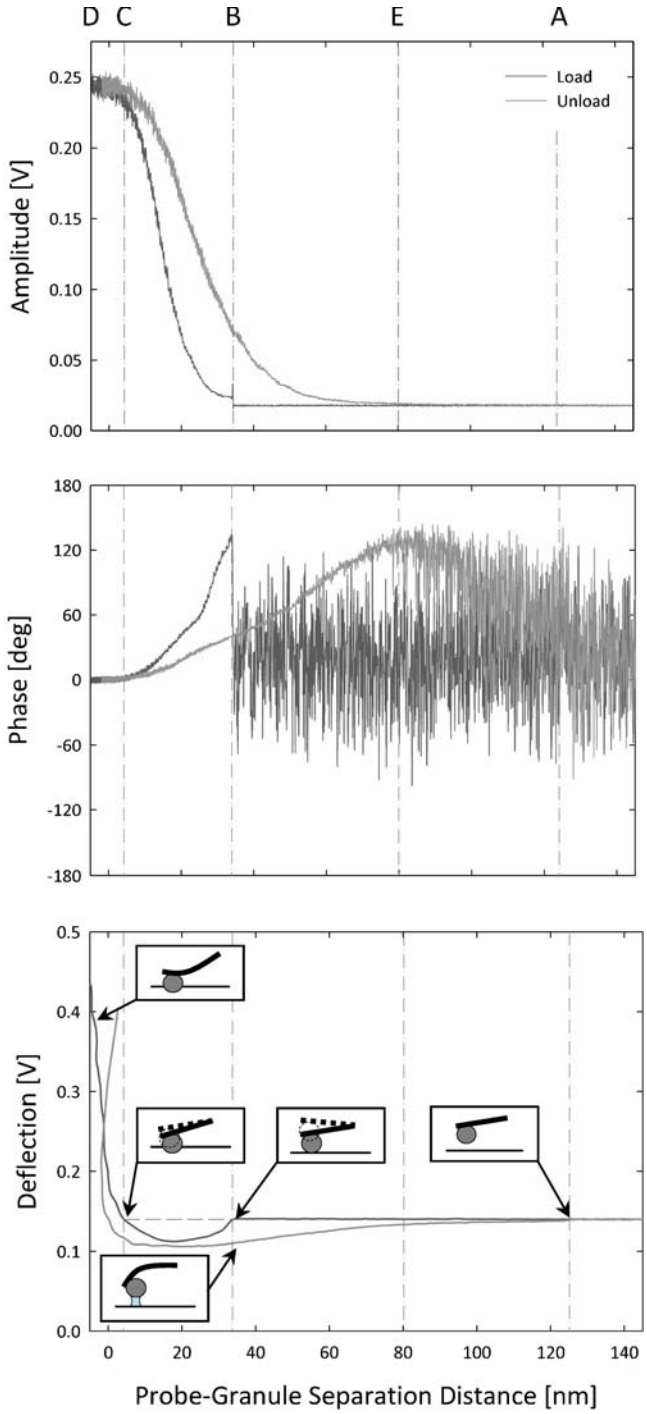

Fig. 7. Overview of an APDD curve.

As the probe withdrew from the granule, G' of the material bridge sharply decreased while G'' initially increased gradually to a maximum value at which it exceeded G' before decreasing again upon rupture (Fig. 8). At the crossover point, where the loss tangent equalled 1 (Fig. 8: ~13 nm), the magnitude of the amplitude signal was low due to weak piezo–cantilever coupling as a result of being connected by a bridge weakening under extension. The deflection signal illustrates that the probe was still in contact with the granule surface and the signal-to-noise ratio of the phase signal was still high; therefore the model is valid at this point (Fig. 8). However, when the withdrawing probe reached the dashed line (Fig. 8) despite the continued, though weak, adhesion the limits of the instrumentation were reached, as insufficient piezo–cantilever coupling existed to adequately characterise the rheology of the bridge. The dashed line was therefore taken as the point of bridge rupture.

When the probe was in full contact with the granule the loss tangent (tan δ) was zero implying the granule surface behaved as an elastic solid, and as the probe withdrew from the surface the bridge properties became less elastic and more liquid-like (Fig. 8). Bridge length appeared to increase with increasing oscillation frequency (Fig. 9). In addition, the gradient of the tan δ curves from the crossover point onwards decreased with increasing frequency.

Comparing the loss tangent profiles for granules made with different grades of PVP it may be seen that bridges containing the higher molecular mass grade (K90) extended to a much greater length before rupture (Fig. 9). Bridges containing PVP K90 appeared to be more elastic in structure when adhesion was at a maximum as the larger molecular weight polymer (K90) behaved more elastically at low levels of extension (Fig. 10). The effect of oscillation frequency on the loss tangent of the probe–granule bridges, measured at maximum values of adhesion at 80% RH, is also illustrated in Fig. 10; increasing strain rates augmented the elasticity of the bridges.

The effect of RH on the G profiles was to decrease the gradient of the adhesion region (Fig. 11). At 20% RH bridge elasticity predominated, where tan δ was less than 1 throughout the whole adhesion event. The length of adhesion measured for both formulations was measured to be within the range of 5–15 nm at all frequencies. This was much shorter than both dynamic adhesion measurements performed at 80% RH, and pseudo static measurements at 20% RH as polymer chains did not have sufficient time to rearrange when subjected to high strain rates. At 80% RH the bridges were predominantly elastic when the distance of separation between the probe and sample was small; however, as the bridge was stretched further, G'' became increasingly dominant and exceeded the G' upon bridge rupture.

DISCUSSION

A disadvantage of applying the Voigt model to measure material bridge rheological properties, as described in this work, lay in the difficulty in accurately measuring probe geometry despite use of a well-defined sphere. The geometry correction factor, b, facilitated the use of AFM deflection data as rheological shear measurements. Two different approximations of b have been previously quoted in the literature (13,14). These different approximations reflect differing physical situations, which are considered below. Radmacher *et al.* (13) have calculated b to be equal to $6\pi R$ (where R is the radius of the probe) based on the assumption that viscous drag imparts a force on the sphere in an isotropic fluid. Montfort and Hadziioannou (14) calculated b for geometries where a sphere located very close to a planar surface experiences a hydrodynamic force dependent on s,

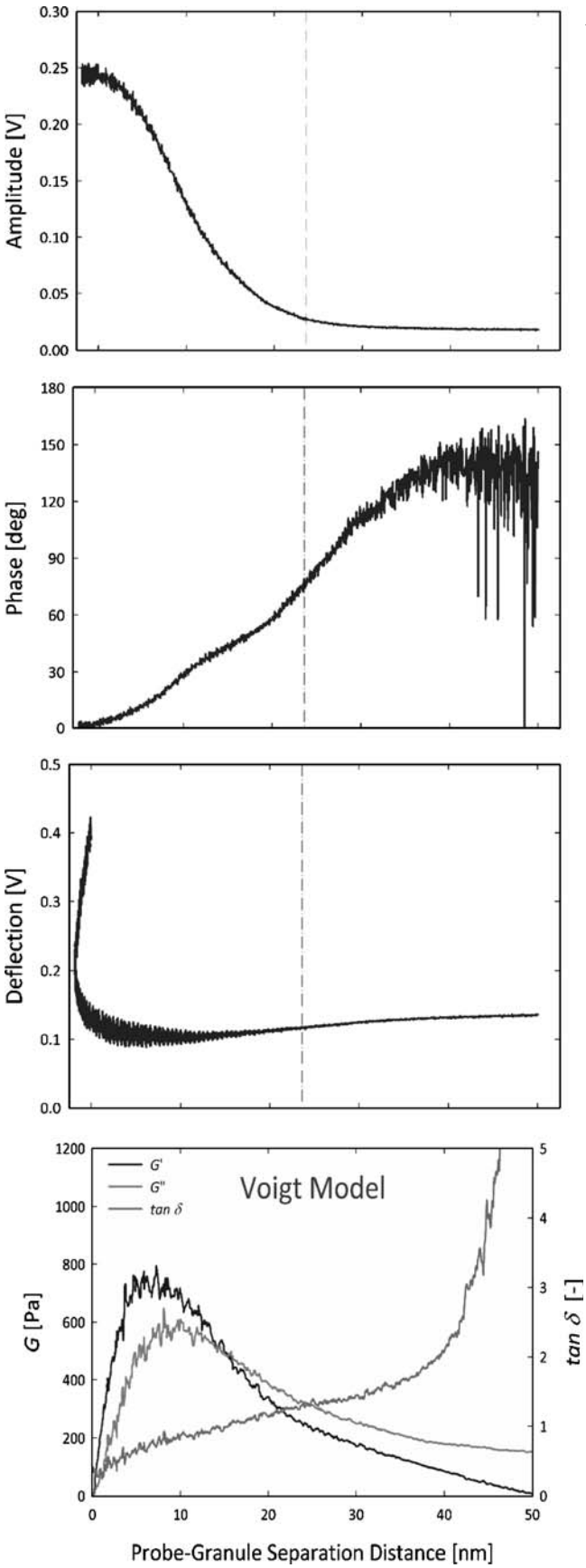

Fig. 8. Conversion of APDD curves to rheological measurement. G', G'' and tan δ profiles of an inter-granular material bridge formed at 80% RH, between a spherical cantilever probe oscillating at 1,000 Hz and the surface of a lactose:PVP K29/32 granule, plotted as a function of probe–sample separation distance and based upon the unload part of the force curve. The *dashed line* represents the boundary of Voigt model; at greater distances of separation amplitude and deflection signals are too low and the signal-to-noise ratio of the phase signal is too high to facilitate accurate measurement of moduli (G). At a distance of 50 nm away from the granule in this instance the G' trace becomes negative and is thereafter meaningless.

the average distance of separation between the sphere and the flat surface ($b=6\pi R^2 s^{-1}$). In the work reported here, even though Montfort's geometry factor was used, neither of these geometries is ideal as the sphere was oscillating in air and was connected to a non-planar surface by a capillary bridge. Choi *et al.* modified Montfort's geometry to account for the contact of two spheres (i.e., $b=1.5\pi R^2 s^{-1}$) (8). Sphere–plane geometry was chosen in this study however, because the true probe-granule geometry was unknown, the radius of the granule surface was unknown, and as the diameter of the microsphere was small (~20 μm) relative to that of the granules investigated

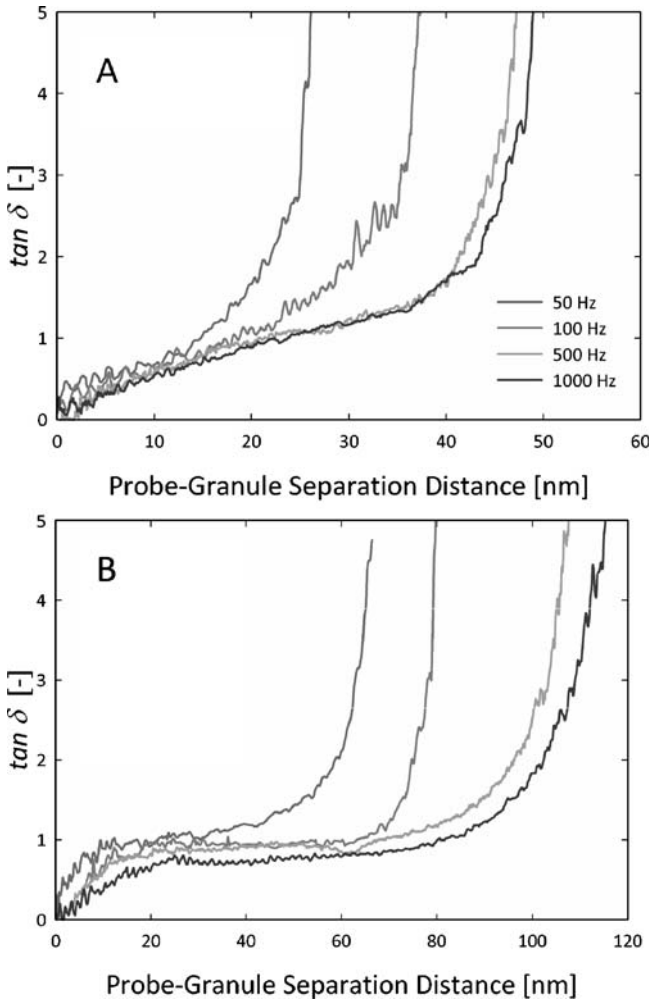

Fig. 9. Effect of oscillation frequency on the tan δ profiles as a function of the probe–sample separation distance for both granule formulations, being lactose:PVP K29/32 (**A**) and lactose:PVP K90 (**B**).

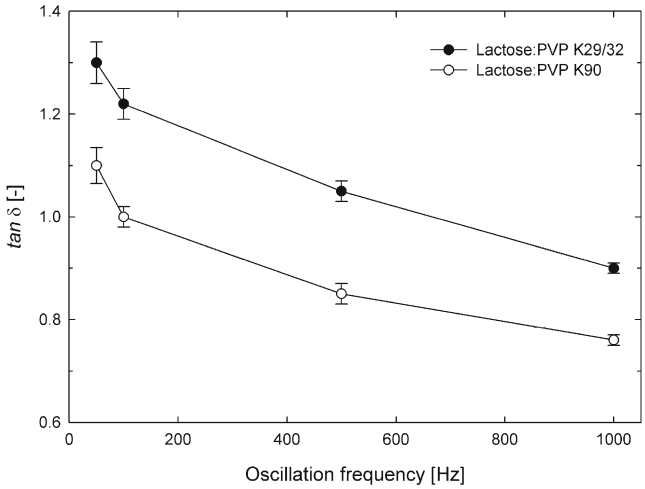

Fig. 10. Effect of oscillation frequency on tan δ values measured at maximum adhesion for both granule formulations.

(>400 μm). Nevertheless, despite issues regarding the geometry correction factor, quantitative analysis of the tan δ, which is independent of b as well as cantilever spring constant (Eq. 3), and qualitative observations of the shear storage and loss moduli may be performed.

The length of the inter-granular material bridge, which underwent the process of dynamic shear, was much shorter than the length of the inter-granular material bridge, which was subjected to pseudo-static extension. This indicates a time-dependency of the polymer properties (Figs. 6 and 9): As might be predicted by normal viscoelastic theory, at high frequencies the behaviour of the Voigt model became more elastic as the motion of the dashpot became negligible in comparison with that of the spring (15). It would be interesting to compare loss tangent values at some reference point further away from the surface. It is, however, problematic to assign such a reference point. This is because it is difficult to identify the exact location of bridge rupture. As the bridge broke the deflection signal indicated relatively low adhesion; low piezo–cantilever coupling existed. This resulted in a minute amplitude signal and a decrease in the signal-to-noise ratio of the phase signal. Nevertheless, at the approximate point of bridge rupture, (Fig. 7 E), the bridge loss shear modulus always exceeded the storage shear modulus at high 80% RH. We hence propose that the crossover point, where G'' equals G', represents onset of untangling of the polymeric binder within the bridge.

This novel technique serves as an innovative method to investigate the viscoelastic behaviour of inter-granular material bridges on a nano-scale. Applying this technique facilitates a fundamental understanding of the rheological properties of inter-granular bridges as they are being sheared at high strain rates. Such information on the deformability of these inter-granular bridges will be useful in predicting and controlling granule growth behaviour in high shear wet granulation.

Future work will investigate the rheology of material bridges composed of different diluents and polymeric binders pertinent to high shear wet granulation.

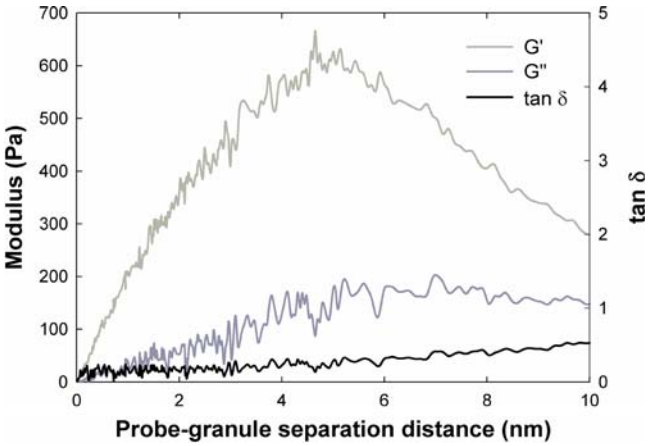

Fig. 11. G', G'' and tan δ profiles of an adhesion event at 20% RH, between a spherical cantilever probe oscillating at 500 Hz and the surface of a lactose:PVP K29/32 granule, plotted as a function of probe–sample separation distance.

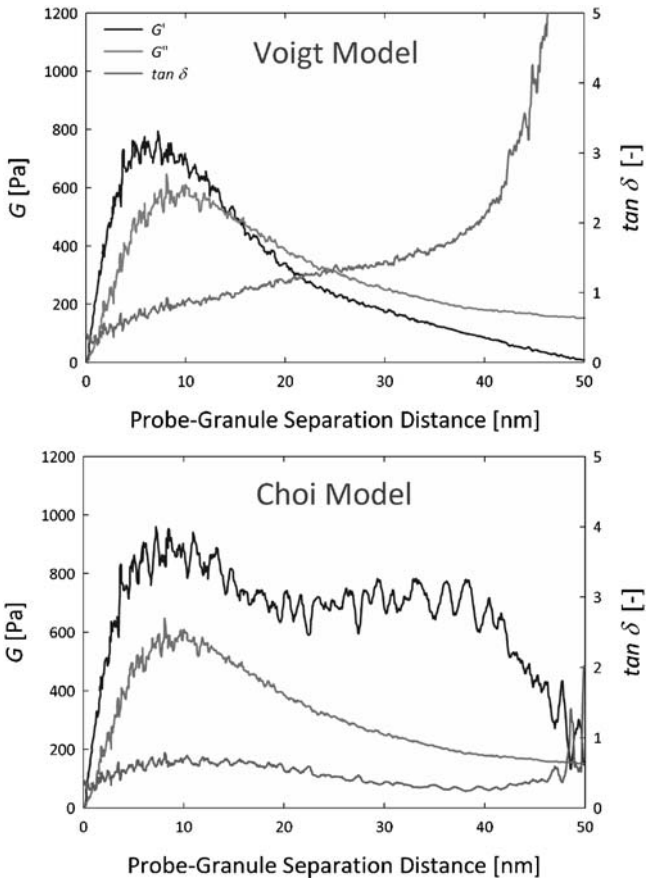

Fig. 12. Conversion of APDD curves to rheological measurement using the Voigt and Choi models. The Choi model accounts for the capillary force of the inter-granular bridge (Eq. 4). G', G'' and tan δ profiles of an inter-granular material bridge formed at 80% RH, between a spherical cantilever probe oscillating at 1,000 Hz and the surface of a lactose:PVP K29/32 granule, are plotted as a function of probe–sample separation distance and based upon the unload part of the force curve.

CONCLUSIONS

AFM has been employed as a rheometer to investigate the rheology of inter-granular material bridges at the nano-scale. This novel method was sufficiently sensitive to discriminate the rheology of two granule formulations comprising polymeric binder of different molecular weight. This method may therefore be used to obtain a fundamental understanding how inter-granular bridges containing different binders, granulated with a diluent, behave at high shear rates.

ACKNOWLEDGMENTS

BC gratefully acknowledges Molecular Profiles for kind use of AFM equipment, Mr Richard Bell, Dr Jonathan CD Sutch and Ms Elaine Harrop at AstraZeneca PAR&D Charnwood for their assistance in manufacturing granules. BC wishes to thank Dr Paul Luckham for insightful discussions regarding this study. Finally, BC thanks AstraZeneca and the EPSRC for funding this studentship.

APPENDIX

Application of the Voigt model in deriving tan δ, G' and G'' values of granular material bridges from dynamic AFM measurements

When the cantilever, driven at a frequency well below its resonant frequency, is not in contact with the substrate it is static, not oscillating and its deflection signal is at the "free level". When the colloid probe of mass m is at the original position it is *static* and experiences no force (Fig. 1: Static state):

$$z = z_0 \tag{5}$$

$$d = z_0 + d_0 \tag{6}$$

where z and d are the piezo drive and probe detected spatial positions respectively, z_0 is the original position of the piezo and d_0 is the cantilever length when static (Fig. 1). It follows that c (cantilever compression or extension) may be defined as:

$$c = z - d \tag{7}$$

In the static state c_0 may therefore be derived as:

$$c_0 = z_0 - (z_0 + d_0) = -d_0 \tag{8}$$

It is noteworthy that Eq. 8 results from defining cantilever compression as positive and extension as negative (Fig. 1). Cantilever extension may also be defined as positive (with compression being negative); this leads to c_0=d_0, without affecting the derivation of rheological parameters.

When the probe is brought into contact with the substrate and the cantilever deflects, the cantilever is in the *pseudo-static* state. The piezo position is equal to its initial position plus its change in position:

$$z = z_0 + \Delta z_0 \tag{9}$$

Similarly,

$$d = z_0 + d_0 + \Delta d_0 \tag{10}$$

and

$$\Delta c = c - c_0 = \Delta z_0 - \Delta d_0 \tag{11}$$

Assuming harmonic oscillation of the piezo, when the probe is in contact with the substrate, and a resultant forced harmonic oscillation of mass m at the same harmonic frequency, the piezo oscillating with an amplitude z_1 drives the cantilever at amplitude d_1. In the *dynamic* state, when the cantilever oscillates, z may therefore be expressed as:

$$z = z_0 + \Delta z_0 + z_1 \times e^{j\omega t} \tag{12}$$

Since the cantilever oscillation lags behind that of the piezo by phase angle θ, owing to the loss component of the sample, d may be written as:

$$d = z_0 + d_0 + \Delta d_0 + d_1 \times e^{j(\omega t+\theta)} \tag{13}$$

and

$$\Delta c = \Delta z_0 - \Delta d_0 + z_1 \times e^{j\omega t} - d_1 \times e^{j(\omega t+\theta)} \tag{14}$$

In addition,

$$\Delta c = \Delta c_0 + c_1 \times e^{j(\omega t+\varphi)} \tag{15}$$

with Δc_0 the DC component of the cantilever deflection, and $c_1 \times e^{j(\omega t+\varphi)}$ the AC component. The phase lag of the deflection signal is denoted by φ. Using Eqs. 7–13 the DC and AC components of the cantilever deflection signal may be separated and cantilever deflection may then be expressed as:

$$\Delta c_0 = \Delta z_0 - \Delta d_0 \tag{16}$$

and

$$c_1 \times e^{j(\omega t+\varphi)} = z_1 \times e^{j\omega t} - d_1 \times e^{j(\omega t+\theta)} \tag{17}$$

Furthermore, the change in position (i.e., the amplitude signal) of the piezo (Δz) and mass m (Δd) is equal to the difference between their position in the dynamic and static states:

$$\Delta z = z_{\text{dynamic}} - z_{\text{static}} \tag{18}$$

and

$$\Delta d = d_{\text{dynamic}} - d_{\text{static}} \tag{19}$$

Therefore,

$$\Delta z = \Delta z_0 + z_1 \times e^{j\omega t} \tag{20}$$

$$\Delta d = \Delta z_0 + \Delta d_0 + d_1 \times e^{j(\omega t+\theta)} \tag{21}$$

Differentiation of Eqs. 12, 13 and 14 yields:

$$\dot{z} = j\omega z_1 \times e^{j\omega t} \tag{22}$$

$$\ddot{z} = -\omega^2 z_1 \times e^{j\omega t} \tag{23}$$

$$\dot{d} = j\omega d_1 \times e^{j(\omega t+\theta)} \tag{24}$$

$$\ddot{d} = -\omega^2 d_1 \times e^{j(\omega t+\theta)} \tag{25}$$

$$\dot{c} = j\omega c_1 \times e^{j(\omega t+\varphi)} \tag{26}$$

$$\ddot{c} = -\omega^2 c_1 \times e^{j(\omega t+\varphi)} \tag{27}$$

Applying Newton's third law of motion, the forces acting on the probe mass m (i.e., the product of its mass and acceleration (Newton's second law) added to the product of the cantilever spring constant and deflection (Hooke's law) is equal but opposite to the force arising from the sample spring and dashpot:

$$m\ddot{d} + k\Delta c = D\dot{d} + K\Delta d \tag{28}$$

where D is the dashpot dampening coefficient and K denotes the spring restoring coefficient.

By substitution:

$$\begin{aligned} -m\omega^2 d_1 \times e^{j(\omega t+\theta)} + k\left[\Delta c_0 + c_1 \times e^{j(\omega t+\varphi)}\right] \\ = j\omega D d_1 \times e^{j(\omega t+\theta)} + K\left[\Delta d_0 + d_1 \times e^{j(\omega t+\theta)}\right] \end{aligned} \tag{29}$$

In AFM, c_1 may be measured directly from deflection signal and z_1 calibrated using a non-deformable elastic surface, but d_1 cannot be measured; substituting for d_1, using Eq. 14:

$$\begin{aligned} -m\omega^2\left[z_1 \times e^{j\omega t} - c_1 \times e^{j(\omega t+\varphi)}\right] + k\Delta c_0 + kc_1 \times e^{j(\omega t+\varphi)} \\ = j\omega D\left[z_1 \times e^{j\omega t} - c_1 \times e^{j(\omega t+\varphi)}\right] + K\Delta d_0 \\ + K\left[z_1 \times e^{j\omega t} - c_1 \times e^{j(\omega t+\varphi)}\right] \end{aligned} \tag{30}$$

In the pseudo-static state, Newton's 3rd Law of motion applies:

$$k\Delta c_0 = K\Delta d_0 \tag{31}$$

If γ is the ratio of c_1 to z_1, and Eq. 29 is divided by z_1 and $e^{j\omega t}$:

$$\begin{aligned} -m\omega^2\left(1 - \gamma \times e^{j\varphi}\right) + k\gamma e^{j\varphi} = j\omega D\left(1 - \gamma \times e^{j\varphi}\right) \\ + K\left(1 - \gamma \times e^{j\varphi}\right) \end{aligned} \tag{32}$$

Dividing by $\left(1 - \gamma \times e^{j\varphi}\right)$:

$$-m\omega^2 + k \times \frac{\gamma e^{j\varphi}}{1 - \gamma e^{j\varphi}} = j\omega D + K \tag{33}$$

$$-m\omega^2 + k \times \frac{\gamma e^{j\varphi}\left(1 - \gamma e^{-j\varphi}\right)}{1 - 2\gamma\cos\varphi + \gamma^2} = j\omega D + K \tag{34}$$

$$-m\omega^2 + k \times \frac{\gamma e^{j\varphi} - \gamma^2}{1 - 2\gamma\cos\varphi + \gamma^2} = j\omega D + K \tag{35}$$

On rearranging, with $e^{j\varphi} = \cos\varphi + j\sin\varphi$:

$$-m\omega^2 + k \times \frac{\gamma\cos\varphi - \gamma^2 + j\gamma\sin\varphi}{1 - 2\gamma\cos\varphi + \gamma^2} = j\omega D + K \tag{36}$$

Splitting Eq. 36 into real and imaginary components:

$$K = -m\omega^2 + k \times \frac{\gamma\cos\varphi - \gamma^2}{1 - 2\gamma\cos\varphi + \gamma^2} \tag{37}$$

and

$$\omega D = k \times \frac{\gamma\sin\varphi}{1 - 2\gamma\cos\varphi + \gamma^2} \tag{38}$$

The mass of the borosilicate microsphere was small: the average mass for the ballotini, with an average density of 2,500 kg m^{-3} and average radius of 10 μm, was 1.05×10^{-11} g. Therefore $m\omega^2 \ll k$ at drive frequencies <1,000 Hz (i.e., at 1,000 Hz: 5.56×10^{-3} N $m^{-1} \ll 40$ N m^{-1}) and it may be assumed that:

$$K = k \times \frac{\gamma\cos\varphi - \gamma^2}{1 - 2\gamma\cos\varphi + \gamma^2} \tag{39}$$

For a sphere–plane geometry Montfort and Hadziioannou (14) derived that:

$$G' = \frac{K}{b} \tag{40}$$

$$G'' = \frac{\omega D}{b} \tag{41}$$

where b, a correction factor used to convert deflection measurements into loss (G') and storage (G'') moduli, is related to the radius of the colloid probe (R) and the distance of separation between the colloid probe and granule surface (s):

$$b = \frac{6\pi R^2}{s} \tag{42}$$

Therefore, by substitution

$$G' = \frac{k}{b}\frac{\gamma\cos\varphi - \gamma^2}{1 - 2\gamma\cos\varphi + \gamma^2} \tag{43}$$

$$G'' = \frac{k}{b}\frac{\gamma\sin\varphi}{1 - 2\gamma\cos\varphi + \gamma^2} \tag{44}$$

The rheological parameter tan δ may be defined as:

$$\tan\delta = \frac{G''}{G'} = \frac{\sin\varphi}{\cos\varphi - \gamma} \tag{45}$$

Comparison of Voigt and Choi models

To allow a comparison between the Voigt and Choi models the experimental APDD data and Voigt derived rheological data shown in Fig. 8 were processed also using the Choi model (Fig. 12). In the case of the Voigt model (Figs. 8 and 12), as the colloid probe moved further away from the granule surface both G profiles decreased. At the crossover point of the G' and G'' profiles, where tan δ equalled 1: distance of separation ~13 nm), the deflection signal illustrates that the probe was still in contact with the granule surface, the signal-to-noise ratio of the phase signal was still high and the amplitude signal was high; therefore the model is valid at this point. In contrast, the Choi model (Fig. 12) which incorporates the elastic meniscus force computed an elevated G'. Whilst G'' decreased with increasing separation, G' remained high and was dominant until bridge rupture. As a result the bridges were predominantly elastic with tan δ being less than 1 throughout. In comparing the models, the peak of the G profiles occurred at the same distance of separation as maximum adhesion (i.e., minimum deflection). Thereafter, traces for G' differ between Voigt and Choi models, however this does not effect the conclusions drawn in this work.

REFERENCES

1. S. M. Iveson, J. D. Litster, K. Hapgood, and B. J. Ennis. Nucleation, growth and breakage phenomena in agitated wet granulation processes: a review. *Powder Technol.* **117**:3–39 (2001). doi:10.1016/S0032-5910(01)00313-8.
2. D. W. York. An industrial user's perspective on agglomeration development. *Powder Technol.* **130**:14–17 (2003). doi:10.1016/S0032-5910(02)00219-X.
3. P. M. McGuiggan, and D. J. Yarusso. Measurement of the loss tangent of a thin polymeric film using the atomic force microscope. *J. Mater. Res.* **19**:387–395 (2004).
4. C. Y. Hui, J. M. Baney, and E. J. Kramer. Contact mechanics and adhesion of viscoelastic spheres. *Langmuir.* **14**:6570–6578 (1998). doi:10.1021/la980273w.
5. G. J. C. Braithwaite, and P. F. Luckham. The simultaneous determination of the forces and viscoelastic properties of adsorbed polymer layers. *J. Colloid Interface Sci.* **218**:97–111 (1999). doi:10.1006/jcis.1999.6298.
6. N. A. Burnham, G. Gremaud, A. J. Kulik, P. J. Gallo, and F. Oulevey. Materials' properties measurements: Choosing the optimal scanning probe microscope configuration. *J. Vac. Sci. Technol. B*. **14**:1308–1312 (1996). doi:10.1116/1.589086.
7. J. W. G. Tyrrell, and P. Attard. Viscoelastic study using an atomic force microscope modified to operate as a nanorheometer. *Langmuir.* **19**:5254–5260 (2003). doi:10.1021/la0207163.
8. J. Choi, and T. Kato. Nanorheological properties of the perfluoropolyether meniscus bridge in the separation range of 10–1000 nm. *Langmuir.* **19**:7933–7940 (2003). doi:10.1021/la034365j.
9. J. E. Sader, J. W. M. Chon, and P. Mulvaney. Calibration of rectangular atomic force microscope cantilevers. *Rev. Sci. Instrum.* **70**:3967–3969 (1999). doi:10.1063/1.1150021.
10. C. T. Gibson, D. A. Smith, and C. J. Roberts. Calibration of silicon atomic force microscope cantilevers. *Nanotechnology.* **16**:234–238 (2005). doi:10.1088/0957–4484/16/2/009.
11. J. K. Eve, N. Patel, S. Y. Luk, S. J. Ebbens, and C. J. Roberts. A study of single drug particle adhesion interactions using atomic force microscopy. *Int. J. Pharm.* **238**:17–27 (2002). doi:10.1016/S0378-5173(02)00055-8.
12. P. M. Young, R. Price, M. J. Tobyn, M. Buttrum, and F. Dey. Investigation into the effect of humidity on drug–drug interactions using the atomic force microscope. *J. Pharm. Sci.* **92**:815–822 (2003). doi:10.1002/jps.10250.
13. M. Radmacher, R. W. Tilmann, and H. E. Gaub. Imaging viscoelasticity by force modulation with the atomic force microscope. *Biophys. J.* **64**:735–742 (1993). doi:10.1016/S0006-3495(93)81433-4.
14. J. P. Montfort, and G. Hadziioannou. Equilibrium and dynamic behavior of thin-films of a perfluorinated polyether. *J. Chem. Phys.* **88**:7187–7196 (1988). doi:10.1063/1.454371.
15. J. D. Ferry. Illustrations of viscoelastic behaviour of polymeric systems, viscoelastic properties of polymers. Wiley, New York, USA, 1980, pp. 33–47.